Chapter 1

Introduction

The first chapter provides an overview of the Sun and its different layers. We also describe the temperature and density structure of the Sun from its core to the outer layer corona. The solar magnetic fields at diverse spatio-temporal scales are briefly described, and thereafter the prominence and its magnetic structuring are delineated. The classification of the solar prominences, their fine structures, and dynamical phenomena are described. This follows a brief review of a variety of magneto-plasma processes, e.g., waves, instabilities, and reconnection, in the solar prominence. A brief introduction is also elucidated about the vortex motion in the prominence. Coronal Mass Ejections (CMEs) and their association with the eruptive prominences are defined. The propagation of CMEs and eruptive prominences, as well as their heliospheric consequences, are finally briefly outlined. We conclude this chapter by outlining the motivation and summary of various original research works carried out in the present thesis. The major scientific rationale and ideas behind these works are discussed in chapters 3-7.

1.1 Overview of the Sun

The Sun is a source of energy for our solar and planetary system, which also makes human life habitable to the Earth. After its formation about 4.6 billion years ago from a cloud of gas, dust, and frozen ice, currently the Sun is considered as a typical magnetically-active, main-sequence star of a spectral class G2V with its average surface temperature of 5800^{o}K. Its absolute magnitude is 4.8. Our star provides a grand cosmic laboratory in our proximity for studying a variety of physical processes and phenomena occurring both in its interior and exterior. The natural plasma processes occur at high energy and large spatial scales at the Sun, which are not possible to achieve in any man-made laboratories in their exact form. The Sun's proximity makes it a unique star to resolve its surface and various layers of the atmosphere for a close enough scrutiny of ongoing dynamical processes there. A variety of scientific studies about the Sun serve as an important guide for understanding the structure and evolution of other stars. The characteristic properties/parameters of the Sun are listed in the Table 1.1.

The solar regions are broadly classified into two major parts, i.e., (i) Solar interior, and (ii) Solar exterior (cf., Figure 1.1). In the interior of the Sun, the dynamics are controlled by the plasma as the plasma β is large there, while in its exterior the magnetic field governs the plasma dynamics in the low β regime. The solar interior is subjected to the thermonuclear reactions in its central core (cf., Figure 1.1). The energy liberated in this reaction is transported upto the Sun's surface by a means of radiative and convection processes, while the neutrinos produced in this reaction do not encounter any hindrance escaping the Sun. The thermodynamical state of the deeper layers of solar interior can be deduced very precisely using helioseismology that utilizes the properties of acoustic oscillations with the period around five minutes. The solar interior also generates the magnetic field most likely at the base of the convection zone in the *tachocline* by the dynamo action. This magnetic

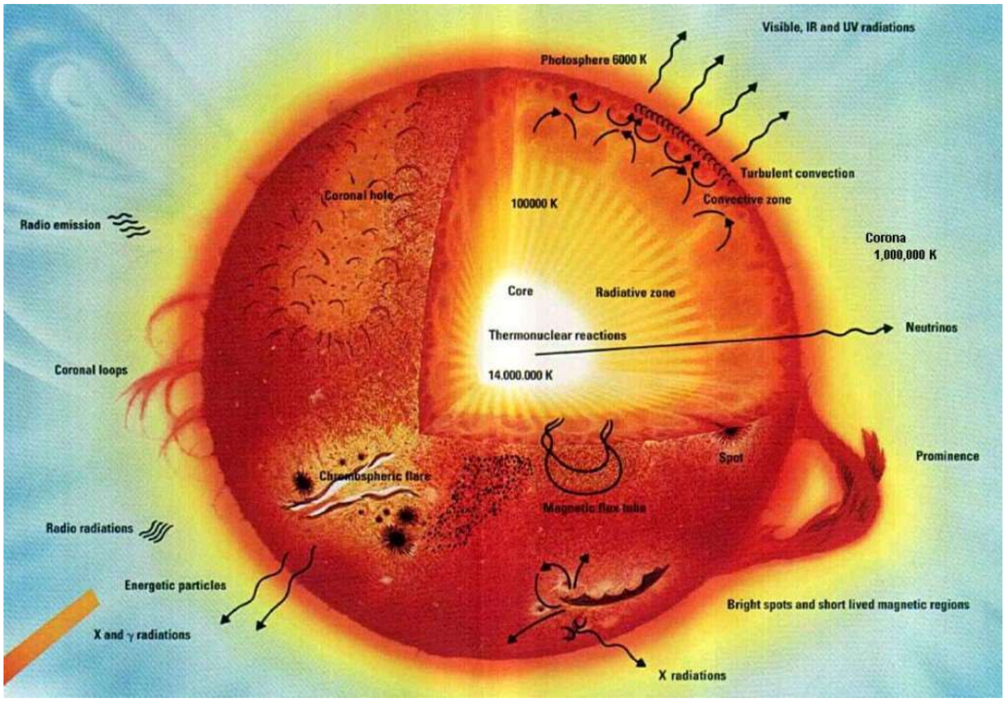

Figure 1.1: The schematic represents the core, radiative, and convection zone in the solar interior, while the photosphere, chromosphere, and corona in its exterior. The thermonuclear reactions and transport of the energy by the mean of radiative and convective motions are illustrated in the interior. General perception of the entire electromagnetic radiations (e.g., γ-rays, X-rays, visible, UV, and radio emissions) are portrayed from different parts of the solar atmosphere. The different magnetic regions (e.g., active regions with the sunspot groups, coronal hole, quiet-Sun) are displayed. The prominence, coronal loops, and magnetic fluxtubes are also shown in the localized solar atmosphere. (Courtesy: www.solarviews.org)

field provides a conduit to transport the energy from powerful sub-surface motions of the Sun and wave activities to the exterior atmospheric layers. At some places in the active regions (ARs) at the solar surface and their overlying atmosphere where the magnitude and complexity of the magnetic fields are already enhanced tremendously, the violent eruptions (e.g., eruptive prominence, solar flares, coronal mass ejections, etc) lead the build-up and release of the magnetic energy in the form of heat and mass motions (energetic particles) at very large spatio-temporal scales and also generate the high energy emissions (X-rays; cf., Figure 1.1). Otherwise, the quiet-Sun (QS) atmospheric magnetic elements comprised by

Physical Parameters	Physical Quantity
Age	4.9×10^{9} year
Mass ($M_{\odot}$)	1.99×10^{30} kg
Radius ($R_{\odot}$)	6.955×10^{5}km
Mean density	1.4×10^{3} kg m^{-3}
Mean distance from Earth	1 AU= 1.496×10^{11}km
Surface gravity (g)	274 s^{-2}
Escape velocity of the Surface	678 km s^{-1}
Radiation Luminosity ($L_{\odot}$)	3.86×10^{26}W
Equatorial (synodic) rotation period	26.24 days
Mass loss rate	1.7×10^{41}kg m^{2} s^{-1}
Effective temperature	5785 K
1 arcsec (1")	≈726 km

Table 1.1: The characteristic physical parameters of the Sun. (Courtesy: Priest 2014)

localized magnetic fluxtubes exhibit the wave dynamics and plasma motions in the form of jets/flows transporting the energy and mass into the overlying solar atmosphere. A brief description of the various layers of solar interior and exterior are described respectively in subsections 1.1.1 and 1.1.2:

1.1.1 Solar Interior

We can not probe directly the interior of the Sun as its internal layers are shielded by opaque plasma beneath the solar surface, i.e., photosphere. However, its physical state can be understood with the help of the governing equations invoking mechanical equilibrium along with the appropriate boundary conditions derived by the observations (Chitre and Dwivedi, 2008; Cox and Giuli, 1968)

$$\frac{dP(r)}{dr} = -\frac{GM(r)}{r^2}\rho(r), \tag{1.1}$$

and

$$\frac{dM(r)}{dr} = 4\pi r^2 \rho(r), \tag{1.2}$$

where $P(r)$, $\rho(r)$, and $M(r)$ are respectively the pressure, density, and mass of the interior of the Sun in spherical symmetry. Since the core generates nuclear energy, therefore, the thermal equilibrium is also maintained by the solar interior by radiating the energy through its surface, i.e.,

$$\frac{dL(r)}{dr} = 4\pi r^2 \rho(r)\epsilon, \tag{1.3}$$

, where ϵ is the generated nuclear energy per unit mass. The $L(r)$=$4\pi r^2(F_{rad}+F_{conv})$ is the luminosity of the Sun, which is the sum of the radiation and convective energy fluxes. The solar interior is classified in the four major layers, i.e., (i) The core; (ii) The radiative zone; (iii) The tachocline region; and (iv) The convection zone. In the following segments, we describe the various layers of the solar interior, and also outline a brief note on the role of solar interior in establishing the solar magnetism

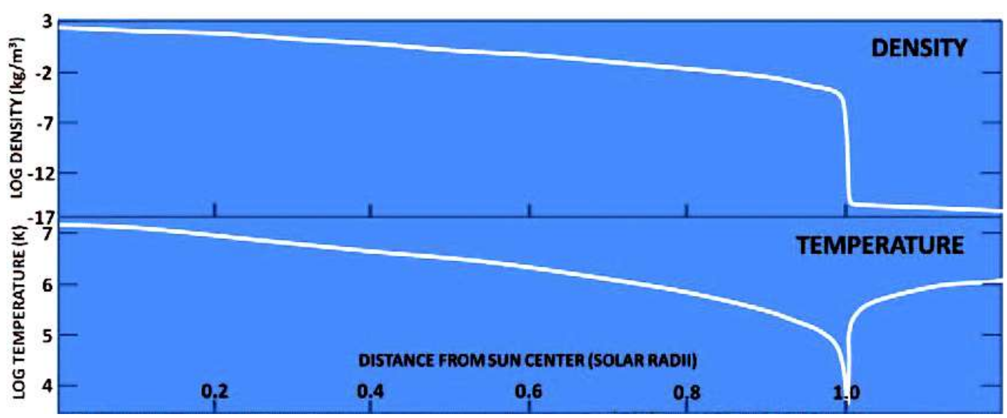

Figure 1.2: Variation of temperature and density with height from the Sun's core to its surface. This image is adopted from Strong et al. (2012). (Courtesy: K. Strong)

The Core:

It is an innermost layer of the Sun where the energy is generated by the nuclear fusion reaction. The temperature of the Sun's core is ~15 million-degree Kelvin, and density is 150 gm cm^{-3}. In the presence of this high temperature and density, the four proton fuse together to form one helium nuclei. This proton-proton ($p-p$) chain is a three-step nuclear reaction that produces elementary particles (e.g., neutrino) and energy of 26 MeV. In this chain reaction, the hydrogen is converted into the helium with ≈0.7% of mass converted into the energy.

$$^{1}H + ^{1}H \rightarrow D + e^{+} + \nu_{e} \tag{1.4}$$

$$D + ^{1}H \rightarrow ^{3}He + \gamma \tag{1.5}$$

$$^{3}He + ^{3}He \rightarrow ^{4}He + ^{1}H + ^{1}H \tag{1.6}$$

The first two reactions occured twice for each occurrence of 3^{rd} reaction → net results.

$$4^{1}H \rightarrow ^{4}He + 2e^{+} + 2\nu_{e} + 2\gamma \tag{1.7}$$

The rate of the fusion reaction at the Sun is 9.2×10^{37} and it generates the energy of the order of 10^{26} Joules per second. At one-fourth of the height of solar radius (1 $R_{\odot}$=6.955×10^{5}km) in the interior, the nuclear fusion reaction is completely stopped. The temperature falls off to 2 MK and density reaches to 20 gm cm^{-3} (cf., Figure 1.2). The 98% of the nuclear energy is generated by $p-p$ cycle in the solar core, while less than 2 % by CNO-cycle. The neutrinos produced in the nuclear reaction move out from the interior of the Sun unimpeded as they do not interact with its opaque matter.

The Radiative Zone:

The radiative zone is lying between $0.25-0.7$ $R_{\odot}$ sandwiched between the outer edge of the core and bottom of the convection zone (cf., Figure 1.1). The energy generated in the core is transferred in form of photons through particle to particle interaction in the radiative zone. The density in the radiative zone falls from 20 gm cm^{-3} to 0.2 gm/cm^{-3}, and a viable temperature gradient sets in (cf., Figure 1.2). The energy is transported in the radiative zone by a mean of radiative processes. In this region, the radiative flux is given as (Chitre, 2003):

$$F_r = -\frac{4acT^3}{3\kappa\rho}\frac{dT}{dr}, \tag{1.8}$$

where a is the Stefan-Boltzmann constant, c depicts the speed of light, while κ is referred as the opacity (Iglesias and Rogers, 1996). Therefore, as stated above that the energy is radiated through radiative processes in this zone and new ionic species start forming by electron recombination of the particles leading higher opacity and temperature gradient. Radiative zone is comparatively denser (cf., Figure 1.2), therefore, the photons generated by thermonuclear reactions at the core travel only a short distance, and they possess very small mean free path. They are absorbed or scattered by ionic species/atoms, therefore, they take a time-scale of million years to travel from the core of the Sun to the top of the radiative zone. In this distance range in the radiative zone, the temperature is also decreased from 15 MK at the solar core to 1.5 MK upto the base of the convection zone or top of the radiative zone (cf., Figure 1.2). The large negative density gradient and inward buoyancy force makes the radiative zone stable and convective motions do not penetrate this zone from the top.

The Tachocline Region:

The convection zone and the radiative zone are rotating differently. Due to the differential rotation, an interface layer is present with a strong shear between these two layers. This sheared region is known as the tachocline region. The plasma motions in the convection zone slowly vanish from the top of this layer to its bottom where the physical conditions match those of the stable radiative zone. The Sun's magnetic field is generated by the differential rotation of radiative and convection zones. The changes in plasma flow velocities across the layer. i.e., the shear flows can stretch magnetic fields to make them stronger. This change in the flow velocity gives this layer its name as the tachocline region. The

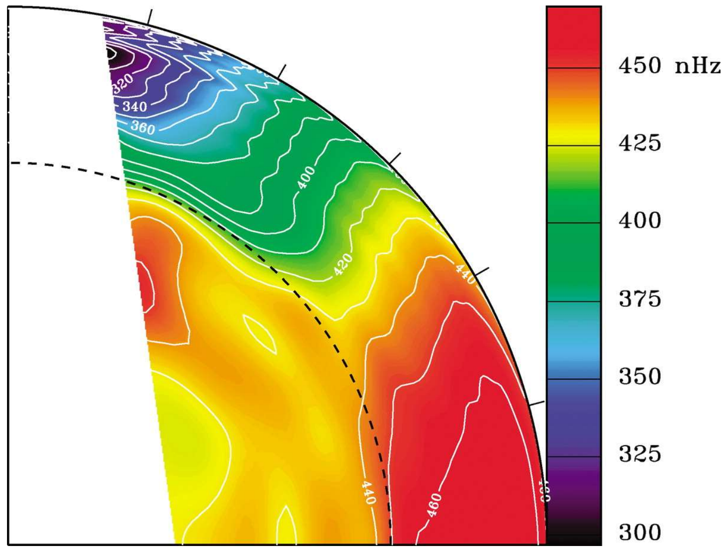

Figure 1.3: Helioseismic measurements determine the internal rotation rate depicting that the longitudinal differential rotation is observed at the solar surface extending through the convection zone. The surface and tachocline regions possess strong radial shear. The blue, green, and red colours represent progressively faster rotations, collectively indicating a solar differential rotation. (Courtesy: NCAR/UCAR, HAO)

sudden changes in the chemical composition also occur across this layer. The shear flow and differential rotation is shown across the tachocline region in Figure 1.3

The Convection Zone:

The collisional ionization is found to be less effective in the convection zone. Temperature falls sharply when we move outward from the center of the Sun. At the base of the convection zone, the temperature is ≈2 MK, which is cool enough for the heavier ions (C, N, O, Ca, and Fe, etc.) to hold some of the electrons in their shells, and it is responsible for the formation of bound-free electrons. This process makes the plasma highly opaque. Therefore, in the convection zone, the radiative temperature gradient rises due to this increasing opacity, and the adiabatic gradient falls off. The radiative temperature gradient is defined as the rate at which it falls with the radial distance. While the adiabatic temperature gradient is the rate at which the temperature radially falls if a volume of material moved higher without adding/losing the heat. The opaque gas traps heat that ultimately makes the fluid unstable and it starts to exhibit the convection. This physical process occurs when the radiative temperature gradient gets larger than the adiabatic temperature gradient, following strictly the Schwarzschild Criterion of the convection (Schwarzschild and Voigt, 1992). These convective motions carry heat quite rapidly to the surface. In such a scenario, the energy flux is transported by convection that is approximated as per a local mixing-length theory (Chitre and Dwivedi, 2008) as follows:

$$F_c = -\kappa_t \rho T \frac{dS(r)}{dr}, \tag{1.9}$$

, where κ_t is turbulent diffusivity, and S(r) is entropy of the system. The plasma expands and cools as it rises via the solar convection towards the solar surface. At the visible surface, the temperature is dropped to 5700 K. The density is only 2×10^{-7} gm cm^{-3} that is almost about 1/10,000th the density of the air at the sea level of our Earth, which indicates ultra-vacuum nature of the solar atmosphere giving rise lots of interesting physical phenomena there. The granular motion, supergranules are the observational manifestations of the convective motion at the visible surface of the Sun (cf., Figure 1.4).

A Brief Note on the Role of Solar Interior on the Sun's Magnetism

To understand the solar interior, its atmosphere, and interplanetary space in connection of the Sun, the basic knowledge of the magnetic field is necessary. The magnetic field is generated due to the differential rotation of the equator and poles of the Sun. This differential rotation appears in the solar tachocline region. The generated magnetic field links the interior of the Sun to the solar atmosphere. The Sun's magnetic field is generated via the dynamo process. The dynamo process can convert the kinetic energy into the electric-magnetic energy. Since the Sun's plasma shows the quasi-neutrality properties (e.g., positive ions, negative ions, and also some neutral atoms), therefore, it is electrically conducting fluid. Such electrically conducting fluids may generate or be affected by the magnetic field. The differential rotation of the Sun shears the electrically conducting plasma at the tachocline region, which amplifies the strength of the magnetic field through the Lenz law. The convective motion and differential rotation get converted into the electric-magnetic energy within the Sun, which suggests that the Sun is a self-sustaining dynamo. The generation of the magnetic field via dynamo processes has been discussed in the following reviews (Charbonneau, 2010; Ossendrijver, 2003; Zwaan, 1987). The magnetic field measurements and challenges in the solar atmosphere is discussed by several authors (Cargill, 2009; Raouafi, 2005; Stenflo, 2013; van Driel-Gesztelyi and Culhane, 2009; White, 2005). The shearing motion amplifies the strength of the magnetic field and produces a very strong localized magnetic field. These localized magnetic fields have enough strength that it can penetrate the visible surface of the Sun (photosphere) and develop the active region where the sunspots are formed. The Sun has an 11-year activity cycle, which is measured in terms of the presence of a number of sunspots on the solar surface (Solanki et al., 2003). At the beginning of the solar cycle, sunspots lie near the mid-latitude region and move towards the equator until the solar minima reach. The movement of the sunspots looks-like a butterfly diagram during 22 years of the complete cycle, which is linked to the sub-surface transport processes. Since solar activity reflects the magnetic activity of the Sun, therefore, several magnetically driven solar phenomena follow this trend. During the solar maxima, the number of sunspots, massive CME eruptions, prominence eruptions, and other large-scale magnetic activities increases. The variation of the solar activity is also related to the variation in the prominence activity (Shimojo et al., 2006). The quiet-Sun also has an ambient field say ~ 5 G. The magnetized plasma erupted explosively due to excess of magnetic energy and cause for small to large-scale eruptions, e.g., solar flares, coronal mass ejection, and may be responsible for the space weather activities. In the next sub-sections, we describe the various layers of the magnetized solar atmosphere and its key magnetic elements.

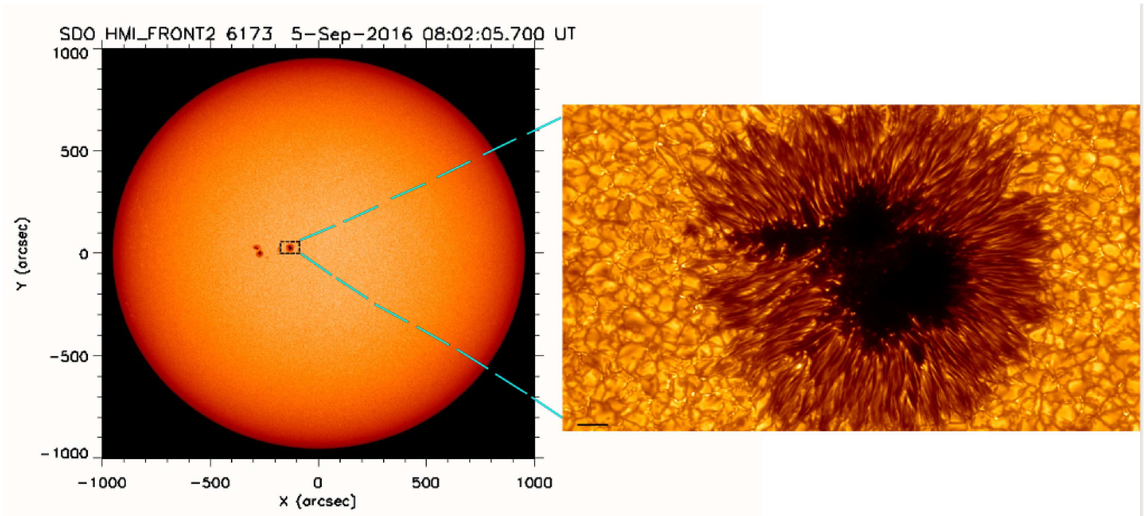

Figure 1.4: The full-disk visible surface of the Sun's photosphere is shown in the left-panel of the image. The zoomed region in right-panel displays the fine details of an active region (AR) sunspot, and the quiet-Sun (QS) granules in its surrounding. (Courtesy: SST; Luc Rouppe van der Voort and Shahin Jafarzadeh, University of Oslo, Norway)

1.1.2 Solar Exterior

The solar exterior is covered by structured (both in density and temperature; cf., Figure 1.2), and magnetized plasma constituting its various atmospheric layers. It consists of a broad range of temperature and density. The solar atmosphere is lying between the solar surface to over millions of kilometers. The innermost layer of the solar exterior is the photosphere, followed by the chromosphere, transition region, and the outermost atmospheric layer corona. The brief description of various layers of the solar atmosphere is given below.

The Photosphere:

The photosphere is a visible surface layer of the Sun, which is a few hundred km wide and emits most of the solar visible radiations as a black-body. It consists of a temperature ranging between 4500 – 6000 K with an average value of 5800 K, and an average density of 3×10^{-7}gm.cm^{-3}. Outside the sunspot regions at the photosphere, it is entirely covered by granules that represent the upper end of the small convective cells (cf., Figure 1.4). In each granule, the central bright region represents the hot upward-moving plasma with velocity 0.5-1.5 km s^{-1}. This upward-moving plasma attains horizontal motion ($\approx$1.0 km s^{-1}) and moves over a typical diameter (0.3-2.0 Mm) in a granule to further cool and sink-down through the darker intergranular lanes. The mean life-time of the granules lies between 5-10 min. At the photosphere, the giant cells of the typical size of 20-70 Mm are also seen through Doppler measurements and are known as Supergranular cells. The plasma flows up at the center of these giant cells with the speed of 30 m s^{-1}, and further moves horizontally outward with the speed of 350 m s^{-1} to fall down through its boundaries (Hathaway et al., 2002). These cells have a lifetime of 1-2 days with a mean of 1.6 days. Some of these fundamental details about solar photosphere are also extensively described in Priest (2014). Apart from granular and supergranular motions, the quiet-Sun photosphere also exhibits the localized vortex motions mostly at the boundary of the supergranular cells (e.g., Bonet et al., 2008). There is an active debate that whether these photospheric vortex motions are associated with the chromospheric swirls/tornadoes and prominence vortices or not (e.g., Panasenco et al., 2014; Wedemeyer-Böhm et al., 2012, and references cited there). The vortex motions of a large-scale prominence and associated dynamical phenomena is also studied in Chapter 4 of this thesis. Using the high-resolution observations, the photospheric bright points are also observed at the supergranular boundaries and their interiors with a typical dimension less than 100 km, and kilo-Gauss (kG) field strength (Priest, 2014; Solanki et al., 2010).

In contrast to the quiet-Sun, the active regions appear at the photosphere and consist of the group of sunspots (cf., Figure 1.4). The dark sunspot is the region of the intense magnetic field about around 1000 Gauss, i.e., in the range of $\approx$1000 – 3000 G. The size of the sunspot lies between 5 Mm and 25 Mm. The temperature of the sunspot lies around 4000 K, which is lower than the average temperature of the solar surface. The life-time of the sunspots may range from several hours to the days during their journey on the solar surface. The central region of the sunspot is termed as umbra which has essentially a vertical magnetic field (cf., Figure 1.4, right panel). Its outer region is known as brighter penumbra in which the magnetic fields have strong horizontal component thus forming the penumbral filaments and canopy. In the photosphere, a small fraction ($\leq 5\%$) of the solar surface is occupied by the active region associated such strong magnetic fields. The plage regions also appear at the photosphere with a typical magnetic field strength of a few hundred Gauss. Plage regions contain a larger area having a magnetic field strength of $\approx$100 – 300 G. Plages with the mixed polarity or unipolarity can also be formed due to strong sub-photospheric dynamics and subsequently the emergence of small-scale magnetic fluxes. The newly developed sunspots which do not possess penumbra, also appear around active regions at the solar photosphere. These structures possessing vertical magnetic fields are known as magnetic pores with a typical size of few megameter and life-time of few hours. The small-scales pores region contain the field strength of $\approx$1000 G. In conclusion, the solar photosphere consists of a variety of magnetic structures at a diverse spatial scale and the strength of magnetic fields, and it exhibits a range of exotic dynamical phenomena, plasma motions, and radiative processes.

The Chromosphere:

The solar chromosphere is the second layer of the solar atmosphere, which lies just above the photosphere and extends approximately upto 2000 km above it. At the bottom of the chromosphere, the temperature minimum of the Sun ($\sim 4.3 \times 10^3$ K) appears. Later, the temperature subsequently increases with a height from 4300 – 25000 K (cf., Figure 1.5).

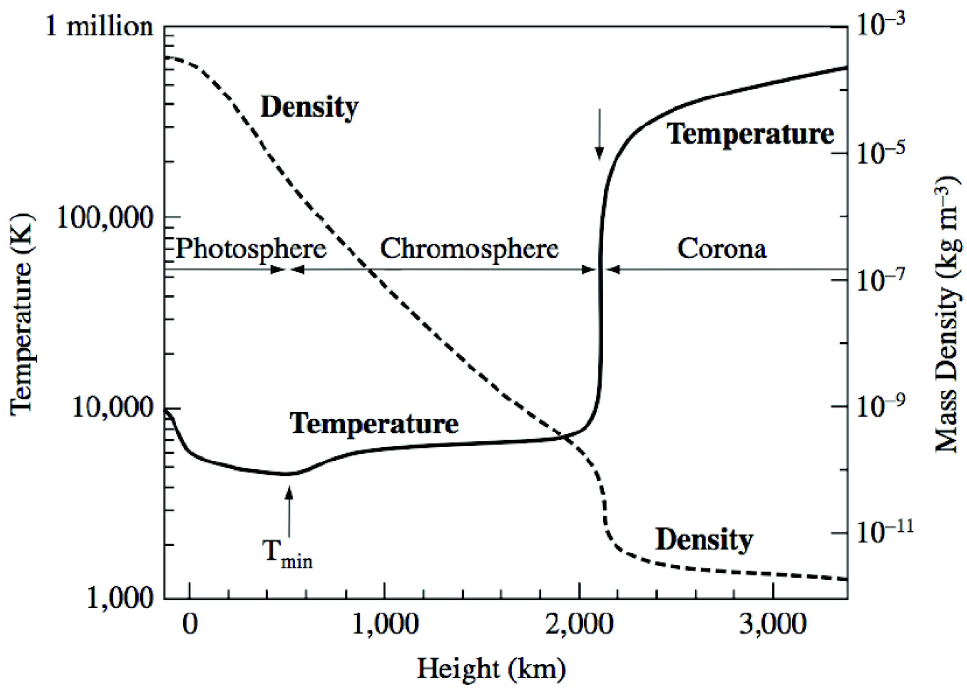

Figure 1.5: Variation of temperature and density with height in the solar atmosphere as per VAL (Vernazza-Avrett-Loeset) solar atmospheric model. (Courtesy: Eugene Avrett, Smithsonian Astrophysical Observatory)

The chromosphere is 1000 – 10000 times less dense than the photosphere. It is a very complex and dynamical layer of the solar atmosphere.

The the Ca II K 3933 Å emissions (cf., right-panel of Figure 1.6) displays the super-granular boundary as an appearance of the magnetic network in the solar chromosphere. These networks are comprised of bright multiple magnetic flux elements hotter than the surroundings. The interior of the supergranular cell manifests as the internetwork in the solar chromosphere where comparatively weaker magnetic fields are present. The internetwork field is a mixed polarity region having magnetic flux strength of 100 – 300 G, and situated in the supergranule interior (Bellot Rubio and Orozco Suárez, 2019; Berger et al., 2004; Rouppe van der Voort et al., 2006; Wiegelmann et al., 2014). The strongly magnetized and localized bright points are also seen in the magnetic networks as an intense

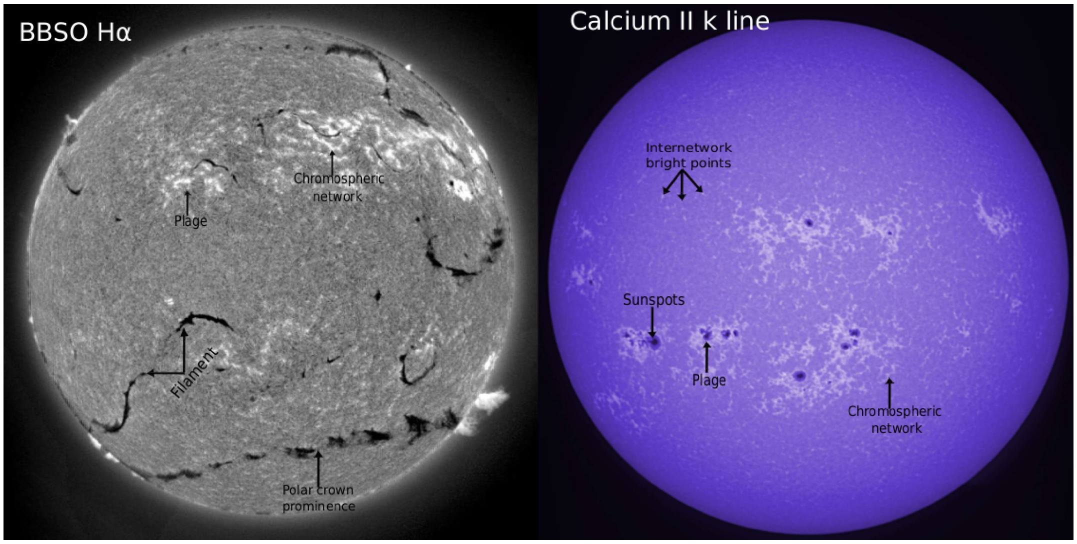

Figure 1.6: The full-disk image of the chromosphere is shown in Hα 6563 Å . Different chromospheric features like sunspots, active regions, filaments, networks, plage regions appear. Right panel: Calcium II K 3933 Å line full disk image of the Sun's chromosphere. Several chromospheric features like sunspots, plage, tiny intra-networks, chromospheric networks, etc. evident in this image. [Courtesy: William Lee (https://www.cloudynights.com/gallery/member/25174-bill-lee/)]

magnetic element of few kG (cf., right-panel of Figure 1.6). The quiet-Sun occupies most of the region of the solar surface and contains the most part of solar magnetic fluxes (e.g., de Wijn et al. 2009).

In Ca II K image, the appearance of magnetically intense sunspots and bright plage regions are also there in the solar active regions. Hα 6563 Å emissions (cf., left-panel in Figure 1.6) from the solar chromosphere show the spectacular magnetic structures and plasma dynamics at diverse spatio-temporal scales (e.g., off-limb thin spicules and cool jets, solar prominence and filaments, polar-crown filaments, bright plage regions, etc). This indicates that the chromosphere is the place where a variety of the indicators are present whose long-term variations reveal the magnetism of the Sun interlinked with the sub-surface transports (e.g., polar crown filament, plage, etc). It is also a highly dynamic portal that plays an important role in supporting the energy and mass transport processes (e.g., waves, shocks, flows/jets, reconnection enabled heating etc) to heat itself and the inner corona. In the present thesis, we focus on understanding some dynamical aspects of solar prominences and their underlying physical mechanisms.

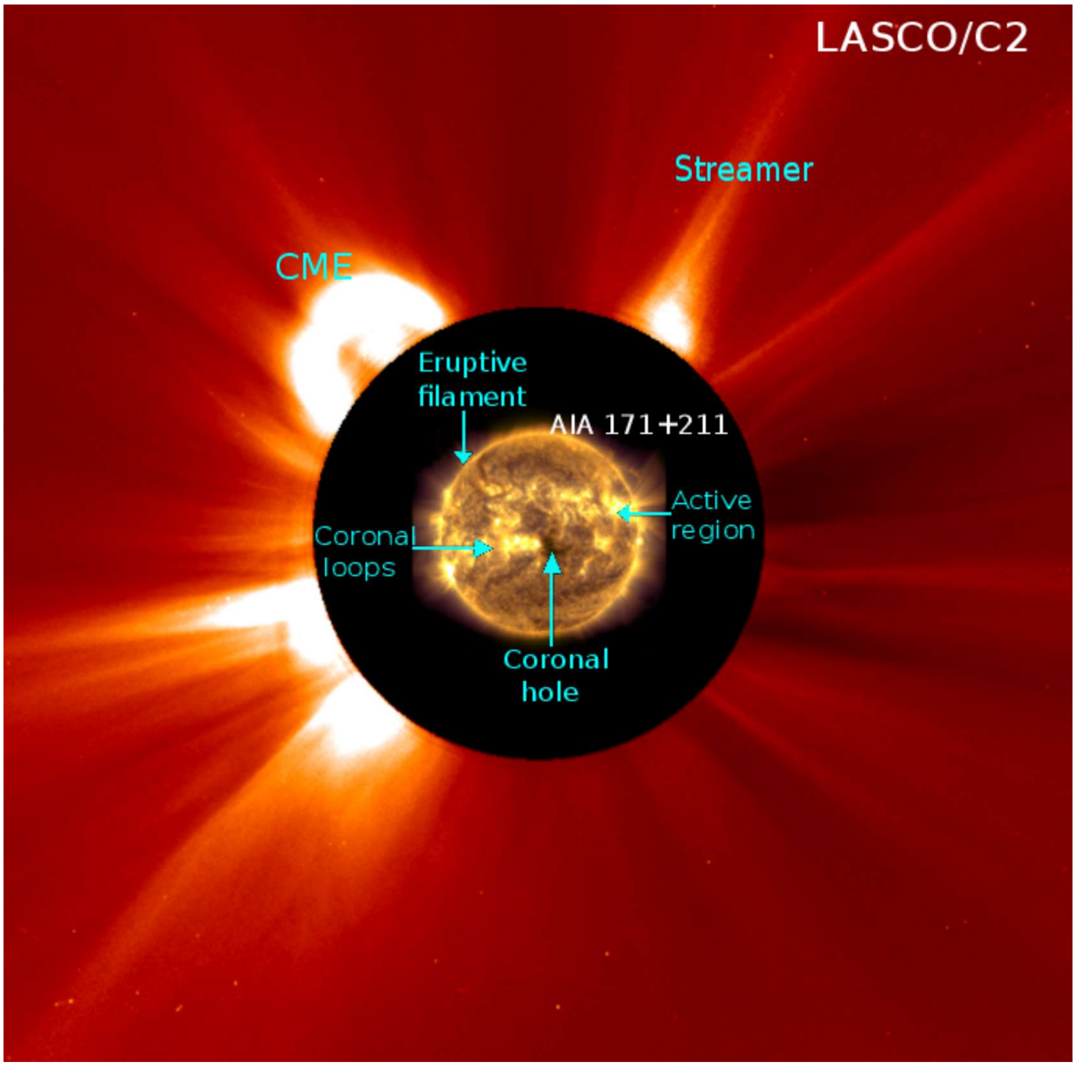

Figure 1.7: The composite view of the EUV inner corona as observed by Solar Dynamics Observatory (SDO)/Atmospheric Imaging Assembly (AIA) 171Å filter and Solar and Heliospheric Observatory (SoHO)/The Large Angle and Spectrometric Coronagraph (LASCO-C2) showing the extended corona upto 6 $R_{\odot}$. Observational data is recorded on 21 April 2015. (Courtesy: SDO/AIA and SoHO/LASCO)

The Transition Region:

The solar transition region is mainly observed in the EUV emissions using space-borne observations. It is a narrow region where temperature rises from $\approx 10^4$ K at its base in the top of the chromosphere quickly upto $\approx 10^6$ K at its top in the inner corona, while density falls rapidly (cf., Figure 1.5). The average height of the transition region varies in various regions of the Sun. For example, its height at 10^5 K in the quiet-Sun may lie in the range of 1700±800 km, while in the coronal hole it may lie much higher spanning between 1500 to 15,000 km (Priest, 2014). This layer acts as an interface between the cool chromosphere and hot corona. A variety of chromospheric dynamical plasma and wave processes encounter through the transition region before they arrive at the inner corona. Coronal thermal conduction and plasma condensation, backward moving plasma in localized magnetic domains, and oscillatory motions coupling the lower atmosphere may also be affected through the solar transition region. These dynamical phenomena witness several discontinuities at the transition region in local characteristic speeds, plasma and magnetic field properties, which affect their dynamics and energetics. Therefore, the transition region acts as a significant layer in determining the mass and energy transport between the chromosphere and corona, and thus regulate the emissions, flows and temperature (e.g., Dowdy et al., 1986; Gabriel, 1976; Jordan, 1980; Peter, 2001; Spadaro et al., 2006, and references cited there).

The Corona:

The word 'solar corona' is derived from the Latin as 'crown of the Sun' (cf., Figure 1.7). It is an outermost layer of the solar atmosphere lying above one million-degree Kelvin temperature (cf., Figure 1.5). In other words, the solar corona is more than three hundred times hotter compared to the visible solar surface (photosphere) beneath it, therefore, it flouts the classical laws of thermal physics and poses a grand challenge to understand the underlying cause for the coronal heating. The temperature of the corona is so high that it consists of fully ionized plasma, and emits predominantly in Ultra-violet (UV)/Extreme Ultra-violet (EUV) and X-rays. It is only seen from the Earth during the total solar eclipse, and more extended corona can be observed and studied by the white light coronagraphs (cf., Figure 1.7). The typical values of the temperature and density in the solar corona can be noted from Figure 1.5. The solar interior and the photosphere are dominated by the plasma pressure, while the coronal equilibrium is governed by the magnetic fields as it possesses high Reynold number conductive plasma. The solar corona consists of mainly three regions, namely, (i) quiet Sun (QS), (ii) coronal-hole (CH), and (iii) active region (AR) (Aschwanden, 2005). Figure 1.7 displays solar active regions with the coronal loops and open magnetic arches, coronal holes, quiet-Sun, and various dynamical phenomena (e.g., eruptive prominences, flows in streamer and coronal rays, etc). A variety of magnetic structures and plasma dynamics in the inner corona are also linked to the magnetic structures (e.g., streamers and coronal rays) and violent eruptions (e.g., CMEs) in the outer corona. Therefore, the corona serves as a platform for the violent solar eruptions, large-scale plasma flows in the form of the solar wind, and various waves and oscillations. The picture of large-scale corona in Figure 1.7 shows the fact that inner coronal dynamics have tie-up at many instances with the dynamics in the outer corona and even in the interplanetary space. Some of the scientific findings in Chapter 6-7 of this thesis will also focus on these aspects of outer coronal dynamics. Since the present thesis studies various aspects of the solar prominence related dynamics, therefore, in the next subsection, we introduce the solar prominence and its magnetic structuring.

1.2 An Overview of the Solar Prominence

Large-scale solar eruptive phenomena (e.g., solar flares, CMEs, eruptive prominences, etc.) are well studied in the Sun's atmosphere and are central issues in the current era

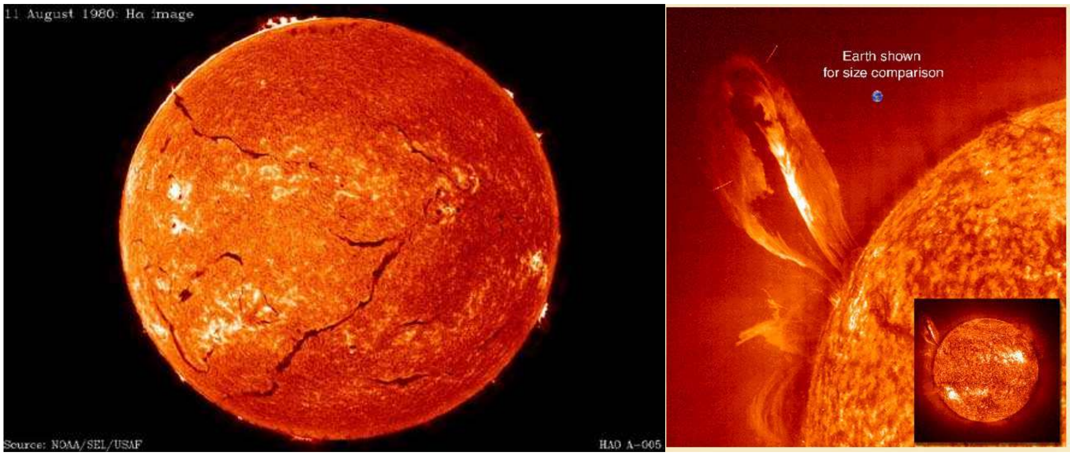

Figure 1.8: Left panel: Large-scale filaments as observed by the Hα filter on the solar disk. Right panel: An eruptive prominence in He II 304 Å with an image of the Earth added for size comparison. (Courtesy: Solar and Heliospheric Observatory *SoHO*/EUV Imaging Telescope *EIT*; Big Beer Solar Observatory)

of solar research due to their connection with the space weather and their influences in the interplanetary space. The prominences, made-up of low temperature, partially ionized, high density, collision dominant plasma, are the most common and complex large-scale eruptive phenomenon in the solar atmosphere. They are cool and dense plasma structures suspended against gravity with the help of the magnetic field lines in the hot solar corona (Labrosse et al., 2010; Mackay et al., 2010; Tandberg-Hanssen, 1998; Vial and Engvold, 2015). They are formed in the chromosphere or in the lower corona above the polarity inversion/neutral line of the photospheric magnetic field (Babcock, 1963; Zirker, 1989). They appear bright on the solar limb in emission due to the higher density as compared to the background corona and known as prominence (cf., Figure 1.8, right panel). However, when they are observed on the solar disk they appear dark due to the high-density background chromosphere and known as solar filaments (cf., Figure 1.8, left panel). Therefore, the name of filament and prominence is interchangeable. There are several interesting scientific problems for the study of solar prominences. The support and stability, internal dynamics, bulk dynamics, magnetic field, formation, and disappearance of the prominence are still-unsettled issues to motivate for pursuing the study about the prominence. Recent high-resolution ground-based observatories (e.g., 1-m Swedish Solar Telescope, Big Bear Solar Observatory Hα observations, etc.) and contemporary space-borne instruments (Hinode, SDO/AIA, Interface Region Imaging Spectrograph, etc.) have confirmed that structural components of the solar prominence are composed of multiple filamentary fine structures (Lin et al., 2005b; Okamoto et al., 2007; Vial and Engvold, 2015). These sub-structures are known as threads and they are the fundamental building blocks of solar prominence. Various models are proposed to support the prominence against solar gravity. The most classical models are, ”normal polarity prominence” and an ”inverse polarity prominence”. Some other most recognized models are “sheared arcade model” (Antiochos et al., 1994; Aulanier and Schmieder, 2002; DeVore and Antiochos, 2000) and “flux rope model” (Dudík et al., 2008; Gibson and Fan, 2006; Kuperus and Raadu, 1974; Low and Hundhausen, 1995; Priest, 1989; van Ballegooijen and Cranmer, 2010; van Ballegooijen and Martens, 1989). Some other most common models are “tangled field model” for hedgerow prominence (van Ballegooijen and Cranmer, 2010) and “flux linkage model” (Martens and Zwaan, 2001) for the development of the polar prominence. A hedgerow prominence consists of multiple vertical threads and they are sustained by the tangled magnetic fields (van Ballegooijen and Cranmer, 2010). The flux linkage model suggests that two unconnected bipoles reconnect due to the flux convergence and reconnection near the polarity inversion line, which creates longer magnetic loops with dips and they are termed as prominence. This process occurred sequentially and is causing for the development of highly sheared longer structures (Martens and Zwaan, 2001). The detailed magnetic structures and their observations are discussed below. Some typical physical parameters of the solar prominences are listed in Table 1.2.

Parameters	**Values**
Temperature	5000-15000 K
Number density	$10^{10}-10^{12}$ cm^{-3}
Magnetic field strength	$4-20$ G
Lifetime	Few hours – few month
Fine structure length (thread)	$3-15$ Mm
Prominence length	$60-600$ Mm
Prominence width	$4-30$ Mm
Prominence height	$15-100$ Mm

Table 1.2: Basic physical parameters of the quiescent solar prominences. The values are adopted from (Lin et al., 2005b; Tandberg-Hanssen, 1995)

.

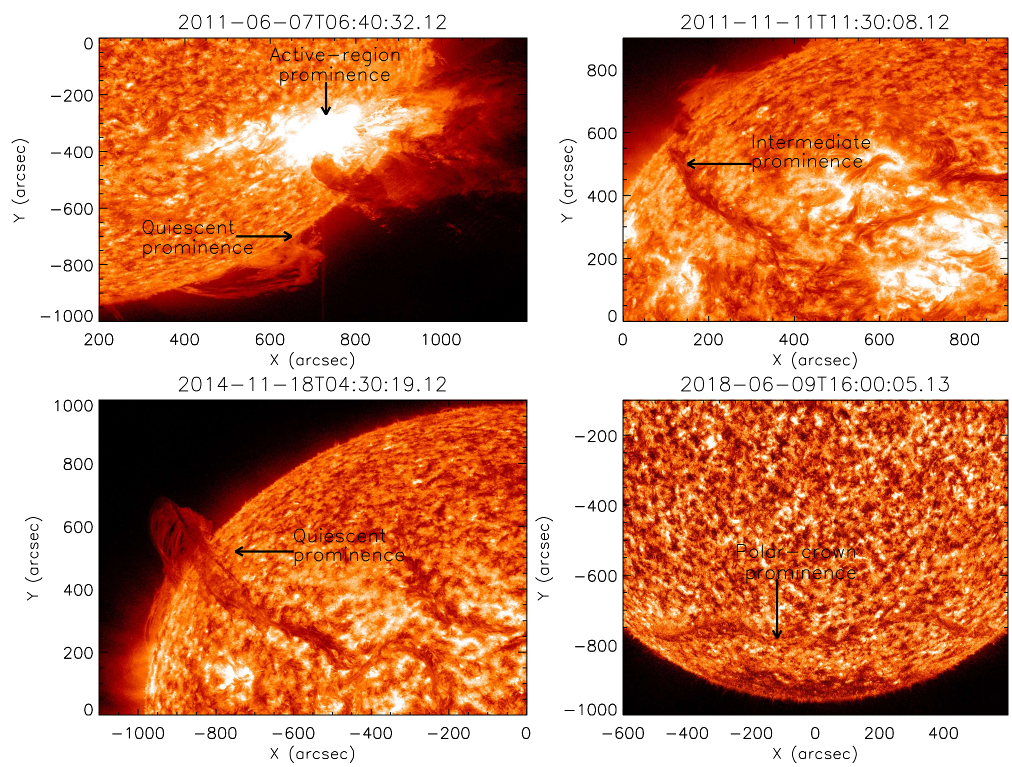

Figure 1.9: Images of the different types of solar prominences based on their location as observed by the SDO/AIA 304 Å filter. (Courtesy: Observational data from SDO/AIA)

1.2.1 Observations of the Prominence

Solar prominences have a long history of observations. The cool prominence material is predominantly made up of hydrogen and helium. Due to the low-temperature in the prominence, it consists of neutral, partially ionized, and collisional plasma inside it. Observations were taken from the different space-borne and ground-based observatories in form of the emission/absorption lines, and they collectively suggest that the prominence has a cool core at chromospheric temperature and a hot envelope maintained at the transition region or inner coronal temperature. Ground-based observations (e.g., DST, SMART, NVST, and SST, etc) have been recorded to observe the cool core of the prominences mostly in the Hα emissions. On the other hand, the space-borne observatories (e.g., SOHO/EIT, SUMER; HINODE/EIS, SOT, STEREO/EUVI, SDO/AIA, and IRIS, etc.) also allow the high-resolution observations of the prominence and Prominence-Corona Transition Region (PCTR). The Ca II H-line (3985.5 Å), EUV He I and He II spectroscopic lines are useful to study the details of the solar prominences. H and He continuum show the absorption behavior when they are observed on the disk in the EUV-FUV range. This absorption feature is used to diagnose the opacity and plasma parameters of the prominence. The prominences are also observed in the microwave and radio wavelengths in the long-wavelength limit. In the microwave range, solar prominence appears bright on the limb as compared to the ambient corona. It appears dark on the disk due to absorption, which is similar to the Hα observations. In radio wavelength range for $\lambda \leq 1$ cm, the core of the prominence is used to be diagnosed. Longer wavelengths can be used to observe the hot part of the prominence, i.e., PCTR. The physical processes involved behind the prominence occurrence, formation, stabilization, and destabilization, is needed to understand both in the prominence core and PCTR in the solar atmosphere. The outer envelope of prominence PCTR is hotter, so it is mainly investigated by the observation of transition region spectral lines. These are the emission lines from the heavier elements, but they still exist in the low ionization state. The PCTR is also easily accessible through the observations of EUV He II 304 Å. The intense gradient of the plasma parameters (e.g., temperature, density, pressure, magnetic field, etc.) at the interface of the PCTR, the prominence may lead to different types of instabilities. They may exhibit several key physical phenomena like internal dynamics, formation and disappearance, support and stability, internal magnetic fields. Such instabilities may also be responsible for their eruption, and sometimes establishing a relationship with the CMEs, etc. The internal dynamics of the prominences and their association with the MHD instabilities is an important issue for solar prominences. Chapter 3 and chapter 6 of this thesis describes the new scientific results obtained on the gravity-driven MRT and KH-RT instabilities occurring in the eruptive solar prominences.

1.2.2 Classification of the Solar Prominences

The properties of the solar prominences vary according to their occurrence, magnetic field structure, and locations, etc. Therefore, they can be classified based on their activity, morphology, location, and magnetic field structuring. The filament/prominence is formed above the polarity inversion line (PIL) separating the opposite polarities of the photospheric magnetic field. Based on the locations, they are classified as (i) Active Region Prominence; (ii) Intermediate Prominence, (iii) Quiescent Prominence, (iv) Polar Crown Prominence.

Active Region Prominence:

The active region prominence is located near the plage regions or inside the active regions (cf., Figure 1.9, top-left panel). The main features of active region prominence are their long thin threads that occur in the horizontal bundles. They are the most violent, short-lived (few minutes to hours), small-scale (10 Mm) prominence, which possesses high magnetic field (20 – 70 G) also as compared to the quiescent prominence. The active region prominences are most dynamical and usually connected more with the large-scale eruptions, like solar flares or coronal mass ejection (CMEs) (Tandberg-Hanssen, 1995).

Quiescent Prominence:

The quiescent prominences generally evolve at the higher latitudes and are associated with weaker photospheric magnetic fields (Priest, 1989). They are long-lived upto a time-scale of few days to months, most stable, and possesss a typical length of $50-600$ Mm and a height of $30-100$ Mm (cf., Figure 1.9, top/bottom-left panel). The quiescent prominence has a relatively low magnetic field (5-20 G) as compared to the active region prominence. The quiescent prominences are formed in the multiple bipolar interaction region (Mackay et al., 2008). Due to bipolar magnetic interactions, the number of the quiescent prominences becomes maximum during the solar maxima and in its decline phase, while minimum during the intermediate time-period of the solar cycle.

Intermediate Prominence:

The intermediate prominences are generally evolved outside of the active regions, generally in the mid-latitude regions between the remnant plages (Mackay et al., 1998). They can share properties of active and quiescent prominence. They form in the multiple thread-like structures (cf., Figure 1.9, top-right panel), which are shorter in length and do not occupy entire PIL (Luna et al., 2012).

Polar Crown Prominence:

Polar crown prominences (PCP) look like the crown of the Sun. They are formed in the northern and southern hemispheres. They appear during the solar minimum and formed in the quiet-Sun. Polar crown prominence consists of multiple threads. The flux-linkage model, in which multiple threads are linked with each other is responsible for the formation of polar crown prominence (Martens and Zwaan, 2001). These multiple threads have a length of 5 – 30 Mm and they act like a pillar to support the prominence (Heinzel and Anzer, 2006; Lin et al., 2005b).

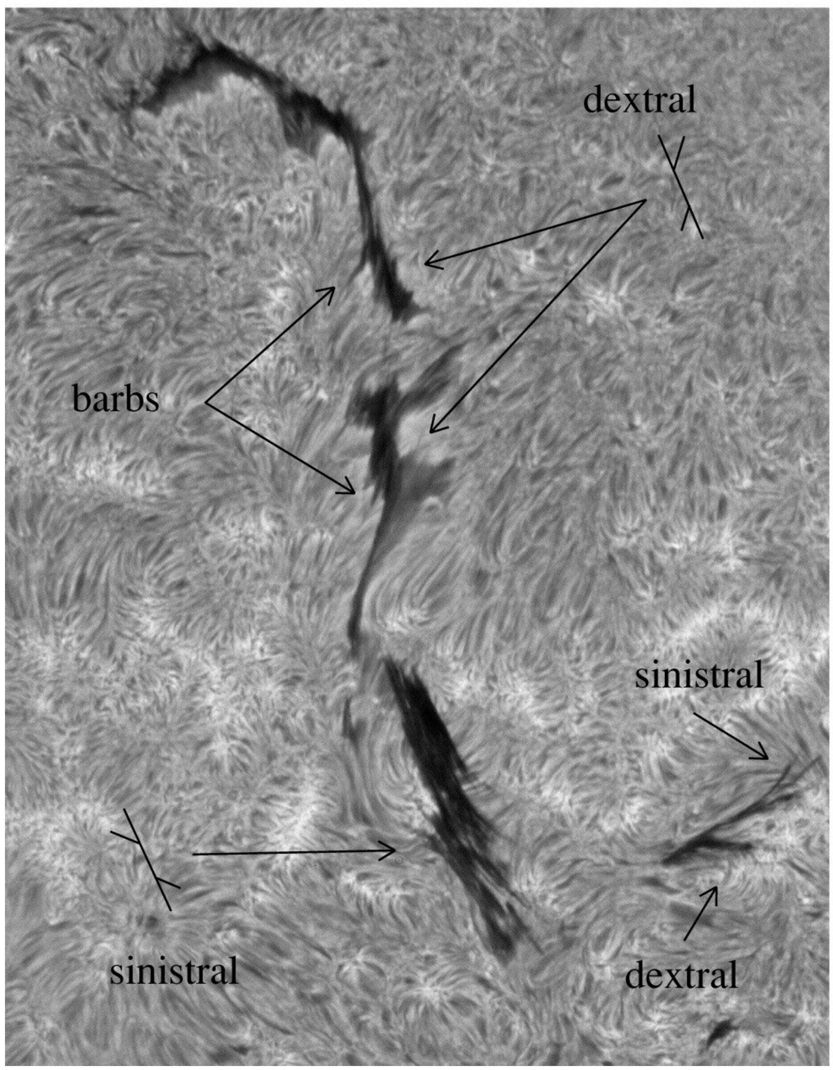

Figure 1.10: A chromospheric filament is observed by the high resolution Hα image on 30th October 2002. Dextral, sinistral, and prominence barbs patterns appear in the prominence. (Courtesy: USAF, ISOON; D. Neidig)

1.3 Dynamics of the Fine-structured Solar Prominences

The morphology and dynamics evolve in a different manner in different solar prominences. These dynamics strongly depend upon the types and magnetic field structuring of the prominence, as well as governed by its fundamental structural components known as threads. The observed dynamics in solar prominence are strongly dependent upon the geometry of the prominence.

1.3.1 Internal Dynamics of the Fine Structures

The prominences have three structural components, i.e., barbs, spine, and two extended legs (Labrosse et al., 2010; Mackay et al., 2010; Martin, 1998; Parenti, 2014). The spines are long horizontal part of the prominence, lying above the polarity inversion line. It connects the two extreme ends of the prominence/filament. The barbs are the vertical components of the prominence and act as a pillar to support the prominence in the tenuous corona (Engvold, 1998). They lie at an acute angle with respect to the prominence/filament (cf., Figure 1.10). High-resolution images of filaments suggest that the barbs make always some angle with the spines (Lin et al., 2008). The beginning and end part of prominence in which the whole prominence is supported is known as extreme ends or prominence legs (cf., Figure 1.10).

The solar prominences/filaments are composed of by the multiple filamentary threads (Lin et al., 2005c; Okamoto et al., 2007; Vial and Engvold, 2015). The dynamics of these threads are very rapid with a lifetime of a few minutes. The size and width (0.15 –0.3") of threads vary rapidly in different types of filaments/prominences. The length of the threads for the spines and barbs may vary and their magnetic field alignment does not necessarily align along the spine (Lin et al., 2008, 2005b). The length of the thread also varies according to the type of the prominences. For active region prominence, the threads are longer for the spine and barbs than the same of the quiescent prominence (Heinzel and

Anzer, 2006). The different lengths of the threads may be caused by the different angles from the filament axis (Mackay et al., 2010). The orientation of the barbs from the filament axis gives the information about the chirality of the prominence. If the movement from the filament axis towards the barbs at an acute angle is clockwise, these types of filaments possess dextral chirality (cf., Figure 1.10). If the movement from the filament axis towards the barbs at an acute angle is counterclockwise, these types of filaments possess sinistral chirality (Martin, 1998; Schmieder et al., 2004).

The solar prominences exhibit several kinds of dynamics such as field-aligned flows and transverse magnetohydrodynamic (MHD) waves (Okamoto et al., 2007) in the horizontal threads, winding motions (Okamoto et al., 2016), large and small amplitude oscillations (Arregui et al., 2012a; Oliver and Ballester, 2002; Tripathi et al., 2009), counter streaming flows (Zirker et al., 1998), different MHD modes (Arregui et al., 2012b; Luna et al., 2018; Zhang et al., 2012), reconnections and heating (Welsch et al., 2005), instabilities (Berger et al., 2011; Innes et al., 2012; Isobe et al., 2005; Mishra and Srivastava, 2019; Mishra et al., 2018a; Ryutova et al., 2010). The detailed description of the prominence magnetic structure and dynamics can be found in (Mackay et al., 2010).

1.3.2 Gravity Driven Instabilities in Solar Prominence

As stated above, the solar prominence also consists of gravity-driven plasma/fluid instabilities (e.g., RT/MRT, K-H instability), as well as they can also possess current-driven instabilities (e.g., kink and sausage instability) and turbulent dynamics at different spatio-temporal scale. The magnetic Rayleigh-Taylor instability and Kelvin-Helmholtz instability are one of the most fundamental instabilities that are gravity-driven. Recent high-resolution observations confirm that these instabilities develop in the solar prominences. These instabilities develop at the interface of two fluids. The magnetic Rayleigh-Taylor instability rises due to the density inversion of two fluids at the interface (cf., Figure 1.11). This insta-

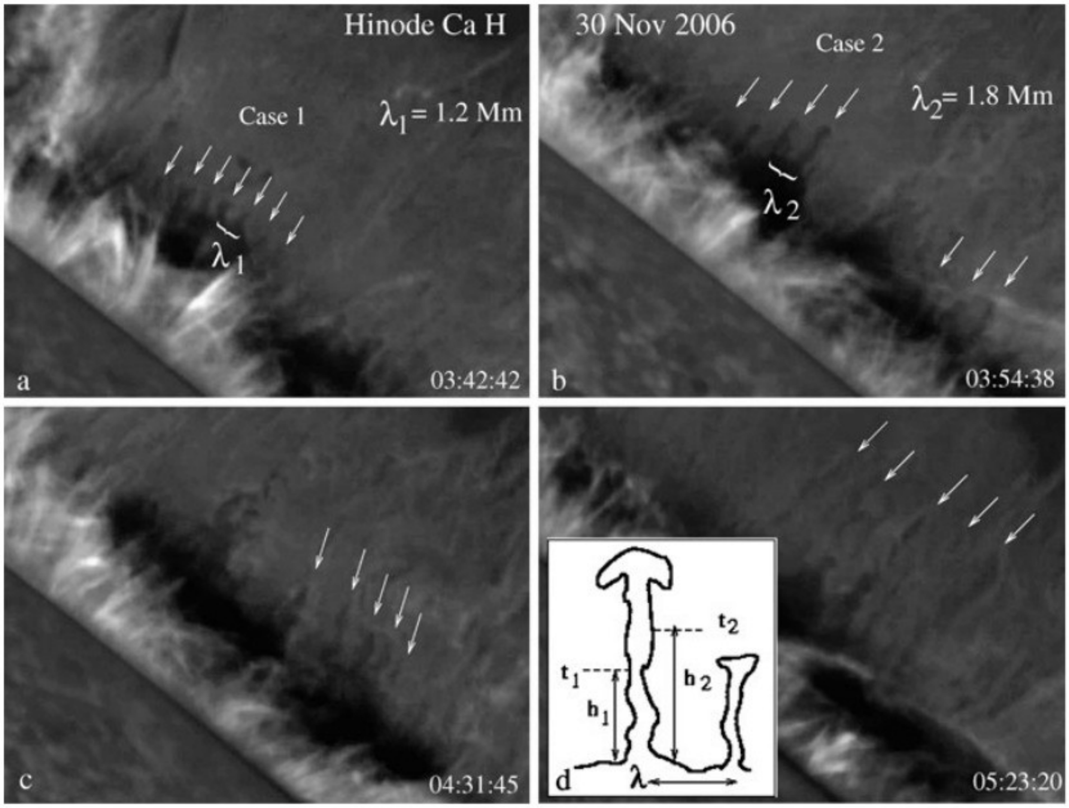

Figure 1.11: Rayleigh-Taylor unstable plumes in a solar prominence in the linear stage with the required conditions, e.g., self-similarity in same family of plumes, similarity of the wavelength/height ratio in different families. Schematic shows the method to estimate the observational growth rate of the instability. (Courtesy: Ryutova et al., 2010)

bility is developed if the low density fluid (ρ_l) lies on the top of the high density one (ρ_h), and accelerated against the gravity. The interface of the two fluids becomes unstable and creates rising and falling plume-like structures. The history of Rayleigh-Taylor instability is more than one and a half years century old. It was first studied by Rayleigh (1882) and later by Taylor (1950) by applying small disturbances at the fluid interface. This instability condition is satisfied when the density gradient of the plasma is opposite to the gravity.

$$g.\frac{\partial n}{\partial z} < 0 \tag{1.10}$$

Linear stability theory is used to understand the exponential growth rate of the fluid-driven instability. The density/pressure gradient is balanced by gravity. The growth rate (γ) of Rayleigh-Taylor instability is,

$$\gamma^2 = -gAk, \tag{1.11}$$

where ρ_h and ρ_l are higher and lower density regions respectively, g is gravity, A is Atwood number that is defined as $A=\frac{(\rho_h-\rho_l)}{(\rho_h+\rho_l)}$, and k is the wave vector. The growth rate of MRT instability is greatly modified by the presence of magnetic field. The generalization of the Rayleigh-Taylor instability from hydrostatic to hydromagnetic conditions in the astrophysical plasma in the presence of magnetic field is known as Kruskal-Schwarzschild instability (i.e., $k \cdot B = 0$) and Parker instability (i.e., $k \cdot B \neq 0$). The presence of magnetic field provides positive support to stabilize the instability. The prominence is cool and dense plasma suspended against gravity in the rarefied corona and possess Rayleigh-Taylor instability. The Kruskal and Schwarzschild (1954) were used to investigate the prominence model, where the mass of the prominence is supported by the tension component of the Lorentz force. Growth rate of the magnetic Rayleigh-Taylor instability became more generalized in the presence of the magnetic field and it is given by Chandrasekhar (1961),

$$\gamma^2 = -gk\frac{(\rho_h - \rho_l)}{(\rho_h + \rho_l)} + \frac{B^2k^2cos^2\theta}{2\pi(\rho_h + \rho_l)}, \tag{1.12}$$

Another gravity-driven fluid instability is the Kelvin-Helmholtz (K-H) instability that develops at the interface of two fluid if there is a velocity gradient ($v_1 \neq v_2$). The flow speed of the upper fluid (v_1) would have to exceed the Alfvén speed (v_2) of the second fluid at the interface to produce a Kelvin-Helmholtz instability. This condition was firstly investigated by Priest (1978).The surface mode of KH instability has been observed in many solar eruptions. The KH unstable vortex is formed at the base of a fast erupted CME (Ofman and Thompson, 2011), on the flanks of CME (Foullon et al., 2011, 2013; Möstl et al., 2013), at the point where emerging flux interacts with the prominence (Berger et al., 2010; Hillier et al., 2017; Ryutova et al., 2010), and sinusoidal-mode in a prominence (Hillier and Polito, 2018).

These above mentioned dynamical phenomena are significant physical processes and provide clues about the complex motions of the prominence. This thesis is focused on some complex dynamics of the eruptive prominences from the lower to the extended corona and also interplanetary space. These peculiar dynamics are, e.g., the evolution of MRT/RT and K-H instabilities in the inner corona; MRT instability and its non-linear evolution in the outer corona; large-scale vortex motion and plasmoid enhanced reconnection within the prominence; prominence driven forced magnetic reconnection in the large-scale solar corona, and an eruptive coronal prominence channel (CPC) and its response in form of coronal jets and geo-effective stealth CMEs. The internal dynamics of solar prominences and their association with the instabilities is an important issue in solar physics. These instabilities also play a crucial role in the prominence formation (e.g., thermal instability), associated internal dynamics and changes (e.g., magnetic Rayleigh-Taylor, Kelvin-Helmholtz instabilities) and its eruptions. These instabilities can be used as a tool to understand the internal plasma and magnetic fields of the prominence. In the present thesis, we study the gravity-driven instabilities (MRT and KH-RT) in different solar prominences (cf., Chapter 3 and 6). The instability driven eruptive prominences may further form the coronal mass ejections, which may be geoeffective as well. Magnetic reconnection is found to be overall a major candidate for the occurrence of the solar eruptive phenomena (e.g., eruptive prominences, solar flares, and CMEs). In the forthcoming two sections (Section 1.4 and 1.5), we briefly describe these two phenomena.

1.4 A Brief Overview of Magnetic Reonnection Process in the Sun's Atmosphere

Magnetic reconnection is a fundamental process, which is important to understand the evolution and dynamics of eruptive phenomena in the solar atmosphere, as well as its heating. The solar magnetic field is highly sheared, which leads it to the magnetic reconnection. The magnetic reconnection is qualitatively introduced as breaking and reconfiguration of the oppositely directed complex magnetic fields into the more simpler configuration of the magnetic field (cf., Figure 1.12). In this process, the magnetic energy is effectively converted into thermal energy, kinetic energy, and accelerated energized charged particles. It is a basic plasma process and it may occur when the oppositely directed magnetic field lines meet with each other in the presence of high magnetic Reynolds number (R_m) and high resistivity. Such a system is characterized in a more general way by the dominant diffusion term in the induction equation:

$$\frac{\partial \mathrm{B}}{\partial t} = \nabla \times (\mathrm{v} \times \mathrm{B}) + \eta \nabla^2 \mathrm{B}, \tag{1.13}$$

which is characterized with a low Magnetic Reynolds number (Priest, 2014) defined as

$$R_m = \frac{|\nabla \times (\mathrm{v} \times \mathrm{B})|}{|\eta \nabla^2 \mathrm{B}|} = \frac{v_0 B / l_0}{\eta B / {l_0}^2} = \frac{l_0 v_0}{\eta}, \tag{1.14}$$

and with a fact that particular localized magnetic reconnection region follows the non-ideal condition as:

$$E + (v \times B) = \eta j. \tag{1.15}$$

Symbols have their usual meaning in the Equation 1.13 to Equation 1.15. The η, j, E, B, v_0, l_0 are respectively the magnetic diffusivity, current density, electric field, magnetic field, velocity scale, and length scale in the magneto-plasma system that undergoes into the

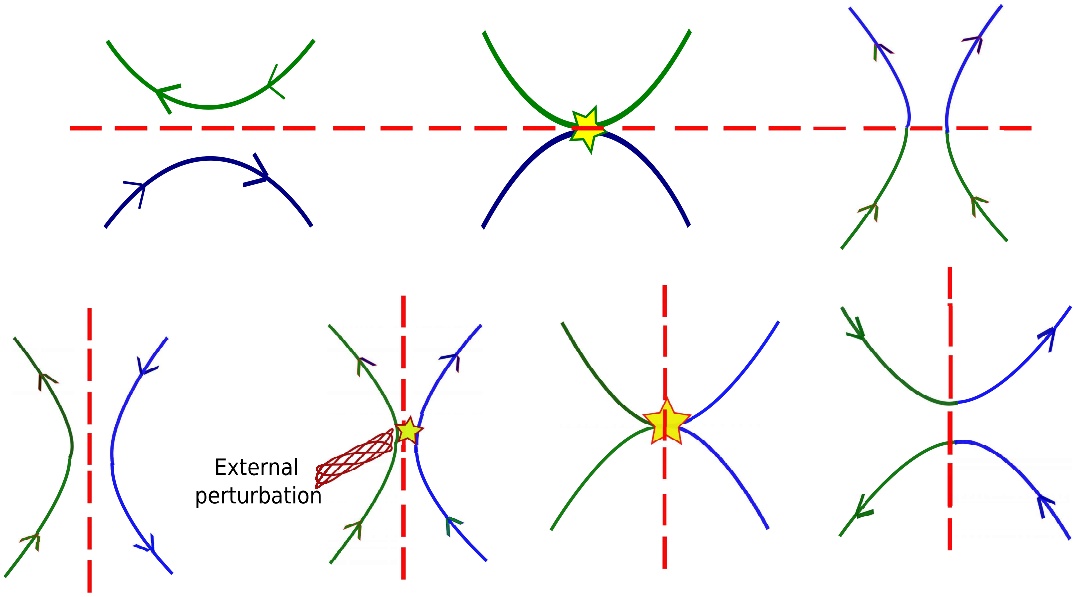

Figure 1.12: Upper panel: A basic schematic that shows the 2D spontaneous magnetic reconnection and release of energy. Different colors show the different connectivity of the field lines and arrows indicate their directions. Bottom panel: 2D schematic for the forced magnetic reconnection. Some external perturbation forced the coronal field lines to reconnect. The spring like structure indicates the external perturbaions and star indicates the reconnection region where the energy release takes place.

magnetic reconnection locally. The following condition depicts the onset of this physical process, along with the Equation 1.15, the following condition depicts the setting in the magnetic reconnection process (Priest, 2014),

$$\eta j \neq \delta v \times B + \nabla \phi, \tag{1.16}$$

where $\delta v = w - v$ in which w is the flux transport velocity in that particular region.

In literature, the term magnetic reconnection is firstly introduced by Dungey (1953). Sweet (1958) firstly introduced the concept of 2D model of magnetic reconnection in the presence of a high Lundquist number having a slow reconnection rate. Petschek (1964) has proposed the concept of fast magnetic reconnection in which a slow shock wave converts the magnetic energy into the heat and kinetic energy. The reconnection rate reaches up to the order of unity. Later, Furth et al. (1973, 1963) have discovered the time-dependent magnetic reconnection triggered by the tearing mode instability. In Chapter 4 of this thesis, we discuss some observational aspects of tearing mode instability in the generation of multiple plasmoids in a twisting and reconnecting solar prominence.

The magnetic reconnection appears in the neutral or current-sheet regions in such a way that the ideal MHD of flux frozen plasma behavior is violated. There exist two possibilities for current-sheet formation during the magnetic reconnection i.e., "free or spontaneous reconnection" and "forced reconnection" (cf., Figure 1.12). In the spontaneous reconnection, some MHD instabilities such as resistive tearing mode (Shibata et al., 1995; Shibata and Tanuma, 2001) or ideal MHD kink mode (Baty, 2000) are responsible for the current-sheet formation. The spontaneous magnetic reconnection plays a crucial role to energize the solar atmosphere. It is one of the strong candidates that heat the corona (Jess et al., 2014; Parker, 1988), small-scale Ellerman bombs (Nelson et al., 2013; Peter et al., 2014; Tian et al., 2016), UV/EUV transients (Innes et al., 1997; Tian et al., 2014), jets (Sterling et al., 2015), large-scale filament eruptions (Schmieder et al., 2013; Xue et al., 2016), solar flares (Masuda et al., 1994; Su et al., 2013), and coronal mass ejections (Savage et al., 2010; Vemareddy, 2017). However, some current-sheets may appear in the MHD stable equilibrium system. Such current-sheets are formed due to forced reconnection in the solar corona (Hahm and Kulsrud, 1985). Some external drivers or perturbations force the system to reconnect and form an elongated current-sheet (cf., Figure 1.12). The solar atmosphere is very dynamic and strongly coupled with the complex magnetic fields. It may appear in a wide range of places, even in a region that has lower resistivity in the solar atmosphere. However, the forced magnetic reconnection only occurs if some external eruptions, displacement in the photospheric foot-points, or newly emerging flux pushes the reconnection process. The theory and model to trigger the forced magnetic

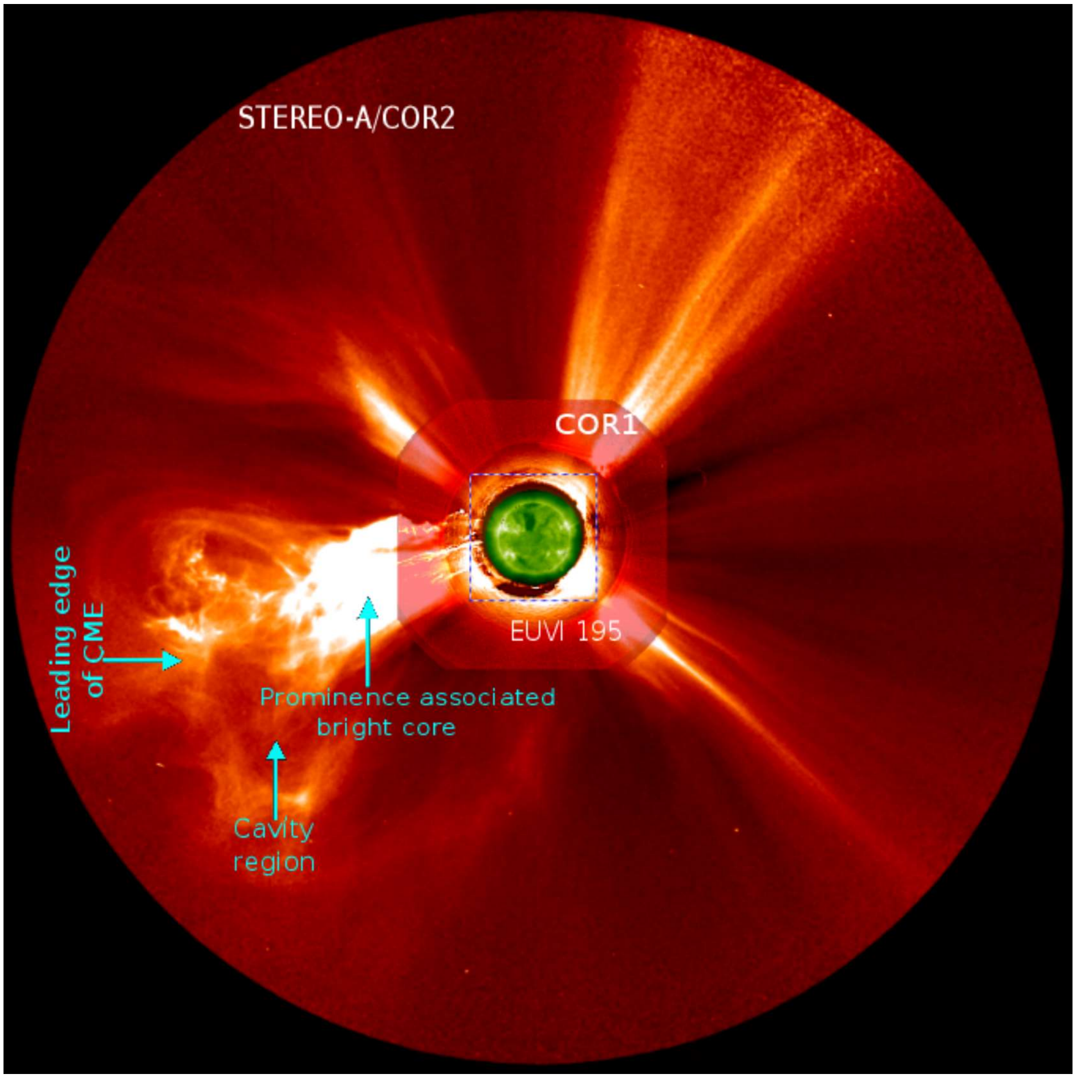

Figure 1.13: CME image is associated with an eruption of the active region prominence on 07 June 2011. The MRT unstable prominence forms the core of CME that propagates in the outer corona. (Courtesy: STEREO/EUVI, COR-I)

reconnection in the solar corona is remarkably developed, e.g., some external perturbation (Hahm and Kulsrud, 1985), nonlinear MHD waves (Beidler et al., 2017; Dewar et al., 2013; Sakai et al., 1984), interfacial perturbations (Fitzpatrick, 2003; Ishizawa and Tokuda, 2000, 2001), the motion of explosive events (Jain et al., 2005; Vekstein, 2017; Vekstein and Jain, 1998), the slow-motion of photospheric footpoints in the coronal magnetic field (Birn et al., 2005; Jain et al., 2005; Vekstein, 2017; Vekstein and Jain, 1998). Although, after the significant development in the theory of forced magnetic reconnection, no direct observational evidence of explosive solar eruptions is reported for the forced magnetic reconnection till the one recently reported by (Srivastava et al., 2019) driven externally by a prominence motion. We describe the observational evidence of "forced magnetic reconnection" driven by prominence in the large-scale solar corona in Chapter 5 of this thesis.

1.5 Coronal Mass Ejections (CMEs) and their Heliospheric Response

Coronal mass ejections (CMEs) are the massive release of magnetized plasma from the Sun into its corona and further into the interplanetary space. They are associated with the solar flares and eruptive prominences (Filippov and Koutchmy, 2008; Gopalswamy et al., 2003; Schmieder et al., 2013; Shibata and Magara, 2011). CMEs are usually observed by using white-light coronagraphic images (cf., Figure 1.13). They generally consist of three structural part, a leading bright edge, lower dense dark cavity region, and a bright core associated with the eruptive prominences/filaments (cf., Figure 1.13). The velocity of the CMEs ranges between $200-3000$ km s^{-1} with an average speed of 500 km s^{-1} (Yashiro et al., 2004). Their mass ranges between $1\times10^{11}-4\times10^{13}$kg with an average mass of 3×10^{12}kg (Gopalswamy and Kundu, 1992). CMEs usually takes $2-8$ days to reach to the

Earth atmosphere and responsible for the space-weather activities (cf., Figure 1.14). The potential role of the CME eruption on geoeffectiveness at the Earth's outer atmosphere is demonstrated in Figure 1.13. Three consecutive CMEs erupted on 22 October 2011, which collectively interact with the Earth's atmosphere on 24-25 October 2011. They exhibit an intense geomagnetic storm (Dst index -146 nT) on 25 October 2011.

In conclusion, in the present thesis, we deal with a variety of physical aspects related to the internal dynamics of the prominences, and the various responses of the eruptive prominences in the inner and outer solar corona. The outline of the thesis is described briefly in the next section.

1.6 Outline of the Thesis

The present thesis describes the followings in the forthcoming chapters:

Chapter 2 deals with the instruments from which the multi-wavelength observational data have been obtained and analyzed for our scientific studies. Various techniques that have been utilized to analyze the imaging data are described.

Chapter 3 presents the observations of MRT-unstable plumes in a loop-like eruptive prominence using SDO/AIA observations. During several key episodes of the internal plasma motions, the signature of the hybrid KH-RT instability is also seen in the prominence. The detailed multiwavelength analyses of the evolution of magnetic Rayleigh-Taylor unstable plumes and hybrid KH-RT instability are described in the observed prominence, and their physical implications are depicted.

Chapter 4 demonstrates an apparent rotating motion in the upper part of an observed prominence. The large-scale vortex motion is also observed in the upper part of the prominence. The slow-motion of the footpoint twists of the prominence due to magnetic shear leads to two different kinds of magnetic reconnection. The internal reconnection is initiated by resistive tearing-mode instability, which leads to the formation of multiple plasmoids

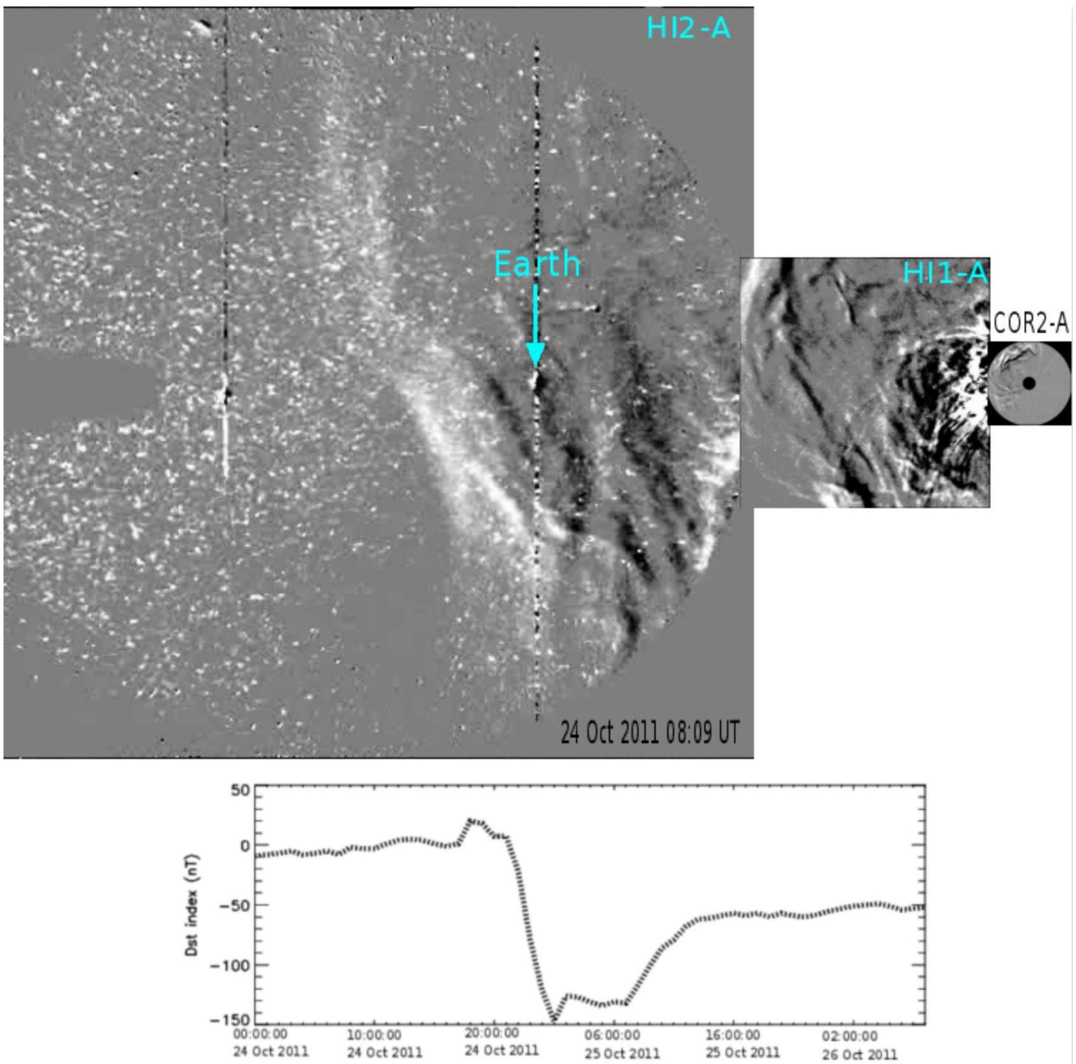

Figure 1.14: Three consecutive CMEs are erupted on 22 October 2011, which collectively interact with the Earth's atmosphere on 24-25 October 2011. They exhibit an intense geomagnetic storm (Dst index -146 nT) on 25 October 2011. (Courtesy: STEREO/COR-II, HI-I)

in the elongated current sheet. While the multiple plasmoid ejections cause the collapse of the magnetic arcades near the X-point and an external reconnection drives further the prominence eruption. In this chapter, the physical significance of the vortex motion and plasmoid ejections in the twisting prominence is established using multiwavelength observations, and their role in the prominence eruption is also discussed.

Chapter 5 describes a novel physical scenario of the formation of a temporary X-point in the solar corona, where plasma dynamics is forced externally by a moving prominence. Natural diffusion was not predominant, however, a prominence driven inflow occurred firstly, forming a thin current sheet and thereafter enabling a forced magnetic reconnection at a considerably high rate. Observations in relation to the numerical model reveal that forced reconnection may rapidly and efficiently occur at higher rates in the solar corona. The physical significance of the forced reconnection is discussed in the large-scale solar corona.

Chapter 6 describes the evolution of MRT instability in an eruptive prominence in the outer corona. In the intermediate corona, the typical plasma structures like fingers, horns, and blobs are seen, which are a typical manifestation of the growth of MRT instability. In the outer corona, the mushroom-like plasma structures have been seen in the unstable prominence segment. These structures are most likely developed due to the breaking and twisting of fingers at large spatial scales in a weaker magnetic field of the outer corona. When the unstable prominence reaches into lower inter-planetary space these structures are fragmented into various small-scale localized plasma spikes most likely due to turbulent mixing. The present work clearly depicts the evolution of the various phases of MRT instability in an eruptive prominence upto the interplanetary space. The physical significance of its various stages has been discussed. The theory of the stability in the magnetized plasma is utilized to diagnose the magnetic field of the outer corona that matches well with the observations.

Chapter 7 describes a linkage of the geoeffective stealth CMEs associated with the eruption of coronal plasma channel (CPC) and a jet-like structure. The CPC represents a coronal counterpart of the on-disk filament. These eruptions launch the CMEs towards the Earth, and upon their arrival the Dst index reaches a negative value of -176 nT and exhibits a strong geomagnetic storm and reduction in the z-component of the interplanetary magnetic field upto -18 nT. The detailed analyses of the various counterparts of the eruption have been analyzed starting from the chromosphere and inner corona to the outer corona. The response of the observed stealth CMEs in creating space weather at Earth is determined and estimated.

Chapter 8 outlines the summary and scientific conclusions derived from the various works conducted during the Ph.D. program. The future prospects of these works are also described.